Journal of Power Sources 195 (2010) 6748–6757

Contents lists available at ScienceDirect

Journal of Power Sources

journal homepage: www.elsevier.com/locate/jpowsour

Effect of material properties on evaporative water removal from polymer electrolyte fuel cell diffusion media

Kyu Taek Cho, Matthew M. Mench*

Fuel Cell Dynamics and Diagnostics Laboratory, Department of Mechanical and Nuclear Engineering, The Pennsylvania State University, University Park, PA 16802, United States

ARTICLE INFO

Article history:
Received 22 February 2010
Received in revised form 28 March 2010
Accepted 29 March 2010
Available online 7 April 2010

Keywords:
Polymer electrolyte fuel cell
Diffusion media
Purge
Evaporation
Capillary flow
Irreducible saturation

ABSTRACT

This work is devoted to delineating the fundamentals of evaporative water removal from diffusion media (DM) to achieve highly efficient and durable gas purge. Multiphase water transport from DM during gas purge is characterized by a balance of internal capillary liquid water flow and water vapor diffusion. In this study, DM with polytetrafluoroethylene (PTFE) content ranging from 0 to 20 wt%, and DM with three different geometric pore structures are utilized to understand this material property effect. It is found that overall evaporative water removal rate increases as PTFE content decreases and as the geometric pore structure changes from a two- to a more three-dimensional structure. This is due to the increase of wettability and porous space favorable for the water transport. The effect of phase-change-induced (PCI) flow and capillary flow on water removal is compared, and it is found that PCI flow is dominant at lower saturation of DM, whereas capillary flow is dominant at higher saturation. The results of this study build upon a previous study by the authors (Cho and Mench [17]), and are useful to understand the competing phenomena of water removal in PEFC DM. The ultimate goal of this work is to guide material design to achieve purge that preserves membrane durability with reduced shutdown power requirements.

1. Introduction

Excessive residual liquid water is known to impede cold start operation and decrease durability of polymer electrolyte fuel cells (PEFC) through a variety of mechanisms, including ionic impurity contamination and carbon corrosion. To minimize the residual water after shutdown, a gas purge is typically applied, due to the simplicity of application [1]. However, the accompanying parasitic energy loss reduces the overall system efficiency. As a result, advanced purge protocols based on the fundamental understanding of evaporative water removal are needed to increase operational lifetime and system efficiency. Although a significant fraction of the overall stored liquid content in a PEFC is known to reside in the diffusion media, very few studies have directly examined evaporative removal from the associated components [2,3].

It is well known that liquid flow inside a DM is affected by wetting properties [4–8]. The DM is generally treated with some hydrophobic polytetrafluoroethylene (PTFE) to improve wet-operation performance. Therefore, the DM has an internal structure of mixed hydrophobic and hydrophilic surfaces, resulting in complicated transport of water. Some fundamental studies of evaporation in porous media have focused on ideal known surfaces such as glass beads. Shahidzadeh-Bonn et al. found the evaporative water removal rate decreased for hydrophobic glass bead porous media due to the poorly developed hydraulic connections among pores [4]. The effect of wettability on capillary liquid transport behavior of DM was evaluated extensively by Kumbur et al. for imbibition [5–7], and recently by Gostick et al. and Fairweather et al. for imbibition and drainage processes [8,9]. They concluded that in materials with hydrophobic treatment, much higher pressure was required for water injection, whereas liquid removal occurred at considerably lower capillary pressures.

Diffusion media are typically manufactured with carbon fibers in the form of the non-woven binder-based substrates or pure woven fabrics. Non-woven DM are categorized into (1) carbon paper DM, with fibers primarily aligned in two dimensions and (2) carbon felt DM, with fibers aligned in three dimensions. The woven DM has well-aligned fibers in a primarily three-dimensional orientation [10]. In previous work, variations of structure were found to significantly alter the amount of stored water in the DM, and the overall cell performance [11–13]. For example, Zhang et al. found from neutron radiography (NR) experiments the water amount stored in carbon cloth was only half of that in carbon paper during fuel cell operation [11]. Kowal et al. also utilized NR and was able to demonstrate that under the conditions tested, paper DM held 174% more water per volume of DM than cloth, and that residual liquid water was more easily removed from the cloth DM. Thus it was concluded that cloth DM is a more effective material for lower power purge [12]. In a modeling study, Wang et al. found that

* Corresponding author. Tel.: +1 814 865 0060; fax: +1 814 863 4848.
E-mail address: mmm124@psu.edu (M.M. Mench).

0378-7753/$ – see front matter © 2010 Elsevier B.V. All rights reserved.
doi:10.1016/j.jpowsour.2010.03.094

Nomenclature

A_s	surface area (m^2)
c	concentration ($kmol\,m^{-3}$)
D	binary diffusion coefficient ($m^2\,s^{-1}$)
J	flux ($kg\,m^{-2}\,s^{-1}$)
M	molecular weight ($kg\,kmol^{-1}$)
m	weight (kg)
$\dot{m}$	mass flow rate ($kg\,s^{-1}$)
N_m	MacMullin number
P	pressure (kPa)
R	gas constant ($kJ\,kmol^{-1}\,K^{-1}$)
r	pore volume ratio of macro-porous layer to total DM
s	saturation
t	thickness (m)
V	volume (m^3)

Greek letters

ε	porosity of diffusion media
κ	permeability (m^2)
μ	viscosity ($kg\,m^{-1}\,s^{-1}$)
ρ	density ($kg\,m^{-3}$)
τ	tortuosity

Subscripts

C	capillary
DM	diffusion media
eff	effective
$evap$	evaporation
imm	immersion
irr	irreducible
l	liquid water
$macro$	macro-porous substrate
MPL	micro-porous layer
p	porous
ref	reference
sat	saturation
t	total diffusion media including macro-porous layer and MPL
w	water

the carbon cloth DM was beneficial for water removal, and consequently is the superior choice for high humidity operation [13]. Stiff paper or felt DM are sometimes preferred by fuel cell manufacturers, however, due to easy of automated stack assembly. However, to the authors' knowledge, fundamental studies to understand the effects of material properties due to the addition of PTFE and geometric pore structure on evaporative water removal in DM have not yet been extensively published.

As recent NR and other studies have revealed, phase-change-induced (PCI) transport is a significant component of water motion during operation and shutdown [14–16]. Neutron radiography is not a dynamic measurement, however, and due to the limited information on actual capillary flow rates in the DM, the competing phenomena for water removal between PCI and capillary transport is not yet clarified.

Evaporative water removal from DM was characterized in detail in a previous study, and a new approach to directly measure the evaporative water removal from DM was developed [17]. Three distinct evaporation regimes were identified: a surface evaporation regime (SER), a constant rate evaporation period (CRP) characterized by capillary flow to the evaporative front, and a falling rate evaporation period (FRP) regime characterized by slower evaporation of separated liquid droplets without internal capillary flow [17]. It has been determined that the dominant water removal mode from the DM during gas purge is changed from liquid-phase capillary transport to vapor-phase evaporative transport below a certain saturation of DM called the irreducible saturation (s_{irr}). To fully understand the water removal behavior from DM, this irreducible saturation point, and the effect of material properties on the saturation point and evaporative motion and removal should be elucidated. Fairweather et al. found water could not be removed from the DM under extremely high external pressure when its saturation level is less than 0.05, and the author concluded s_{irr} should be less than 0.05 [18]. Gostick et al. found that the s_{irr} is 0.07 for SGL 10BA DM and 0.04 for Toray 90 DM [19]. However, none of the previous works focused on understanding the effect of material properties on irreducible saturation.

As PTFE content and pore structure of DM change, the properties of the DM pores are altered chemically (i.e. wettability) and physically (i.e. porosity, permeability, and tortuosity) [8]. It was concluded that changes in DM chemical properties have a dominant impact on capillary liquid transport [8]. The effect of chemical property changes can be investigated in the regime where capillary flow is the dominant mode of water removal. The effect physical properties is dominant in the regime in which vapor diffusion is the controlling mechanism, i.e., below the s_{irr} saturation level.

The objective of this study is to build on and significantly extend the results of our previous study [17], and to define the impact of material properties on water removal behavior during gas purge by investigating the effect of PTFE content in DM with various 2D and 3D pore structures. An analysis of the effects of material properties on evaporative removal is conducted for pendular (diffusion dominated) and funicular (capillary flow dominated) regimes. The effect of phase-change-induced (PCI) flow and capillary flow on water removal is compared to understand the competing phenomena of water removal in DM. Additionally, a new method is developed to measure the irreducible saturation of DM, and the effect of material properties on s_{irr} was investigated. Finally, the potential impact of material PTFE content and structure on purge efficiency is discussed.

2. Experimental

2.1. Porosity measurement and evaporation test

Porosity is a key material property for controlling saturation and multiphase heat and mass transfer in porous media. In this study, the method of immersion imbibition was utilized to measure porosity of tested DM. In this study, five pieces of samples ($8 \times 80\,mm^2$) were die-cut from a sheet of DM material, and their dimensions were measured with a caliper. Then, DM were immersed into the totally wetting fluid (n-hexane) contained in a scaled cylinder (10 mL, Pyrex™), and volume changes before and after the immersion were measured. Porosity of DM was obtained from the following equation:

$$\text{Porosity}\,(\varepsilon) = \frac{\text{pore volume}}{\text{total volume of DM}} = \frac{V_{t,DM} - V_{solid,DM}}{V_{t,DM}} = \frac{V_{t,DM} - (V_{after,imm} - V_{before,imm})}{V_{t,DM}} \quad (1)$$

where $V_{t,DM}$ is total volume of DM, $V_{solid,DM}$ is volume of solid phase in DM, $V_{after,imm}$ is volume of n-hexane after DM immersed, and $V_{before,imm}$ is volume of n-hexane before DM immersion.

Sonic vibration was continuously applied to the cylinder with a sonic cleaner (VWR model 50D) to remove residual bubbles and achieve complete saturation. With this approach, the maximum deviation in measured dry porosity was ±1.6%.

SGL™ Sigracet® 10 series DM with variable PTFE content from 0, 10, and to 20 wt% were utilized to investigate the effect of PTFE content on the water removal. For the comparison of structure,

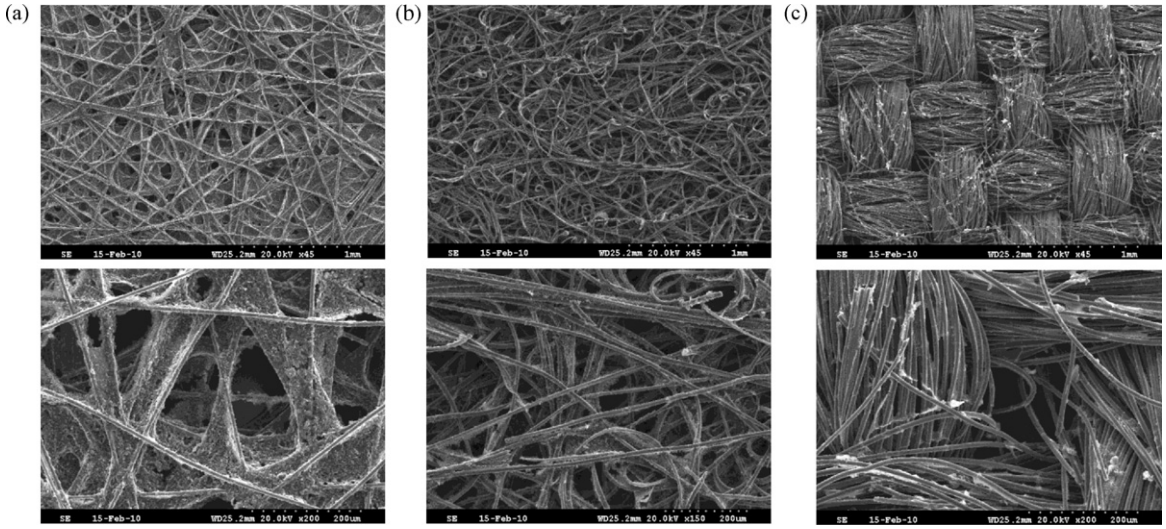

Fig. 1. Comparison of SEM images: (a) carbon paper-type DM (2D pore structure), (b) carbon felt type DM (partial 3D pore structure), and (c) carbon cloth type DM (3D pore structure).

Table 1
Material properties of DM.

DM	Structure[a]	PTFE content[a]	Porosity[b]	Thickness[b] (mm)	Dry DM weight (g)	Weight (g) of water in DM at $s = 0.5$	Macro-porous substrate[b]	
							Porosity	Tortuosity
SGL 24AA	Carbon paper without MPL	0 wt%	0.87	0.18	0.0803	0.1107	0.87	1.48
SGL 10AC	Carbon felt with MPL	0 wt%	0.82	0.37	0.1929	0.2106	0.89	1.39
SGL 10CC	Carbon felt with MPL	10 wt%	0.81	0.37	0.1953	0.2075	0.88	1.43
SGL 10DC	Carbon felt with MPL	20 wt%	0.80	0.38	0.2316	0.2117	0.85	1.58
Carbel CL	Carbon cloth with MPL	N/A	0.75	0.37	0.2317	0.1911	0.82	1.10

[a] Information supplied from manufacturer.
[b] Values measured or calculated in this work.

three different types of DM were selected, based on manufacturer information. A carbon paper-type DM (SGL^{TM} Sigracet® 24 series 24AA), with DM with fibers aligned primarily in a 2D planar direction, a carbon felt type DM (SGL^{TM} Sigracet® 10 series DM 10AC), with fibers primarily aligned in the x and y direction as well as partially in z (through-plane) direction, and a carbon cloth type DM (Carbel CL®), with fibers aligned in 3D direction were selected. SEM images of typical pore structure of DM are shown in Fig. 1. Detailed material properties of the DM utilized are summarized in Table 1.

DM were artificially saturated with de-ionized (DI) water under vacuum pressure, and they were implemented into the experimental apparatus. By applying controlled dry air purge flow rates, water was convectively removed from DM, while the weight change of the DM was measured with an electronic scale. The unique evaporation test setup and methodology were described in detail in Ref. [17].

3. Results and discussion

3.1. Overall behavior of water removal during gas purge

Water removal behavior during gas purge for SGL 10AC, 10CC, and 10DC was compared at gas purge flow rates ranging from 0.25 SLPM to 7 SLPM, as shown in Fig. 2. The flow rates tested correspond to Reynolds numbers from 13 to 370, which is a range appropriate for comparison to normal fuel cell operation in a current density range from 0.05 to 1.50 A cm^{-2}.

All of the tested samples showed similar water removal trends; fast water removal during the initial purge, followed by steady water removal of which the duration was in inverse proportion to the gas purge flow rate, and finally a rapid decrease in the water removal rate after the saturation falls below a critical value. This is consistent with the results in Ref. [17]. Interestingly, total purge time was found to increase with an increase of PTFE content, which is also consistent with some literature [4,20]. This interesting trend is a result of the fact that the PTFE additive promotes transition to a discrete droplet pendular regime, limiting capillary flow. Although the addition of PTFE is beneficial to provide access for gas phase reactant in high-humidity environments, it reduces the capacity for drainage and therefore increases the residual water droplets which must be evaporatively removed during purge or remain in the DM after shutdown.

Water removal behavior was further compared with respect to the normalized water removal rate[1] of Fig. 3(a) and the saturation level of DM of Fig. 3(b), respectively, where liquid saturation of DM was obtained from the following equation:

$$\text{Saturation } (s) = \frac{\text{pore volume filled with liquid water}}{\text{total dry pore volume of DM}} = \frac{(m_{wet,DM} - m_{dry,DM})/\rho_w}{\varepsilon V_{DM}} \quad (2)$$

where $m_{wet,DM}$ and $m_{dry,DM}$ are weight of wet and dry DM, respectively, ρ_w is the density of water, ε is the porosity of DM, and V_{DM} is the volume of total DM.

It was found that with higher PTFE content, the transition from the constant rate period regime (CRP) to the falling rate period regime (FRP) was generated at higher saturation levels, and the

[1] Normalization was performed by dividing with water removal rate obtained by extrapolating the tangent lines from constant water removal region to initial purge time, as described in detail in Ref. [17].

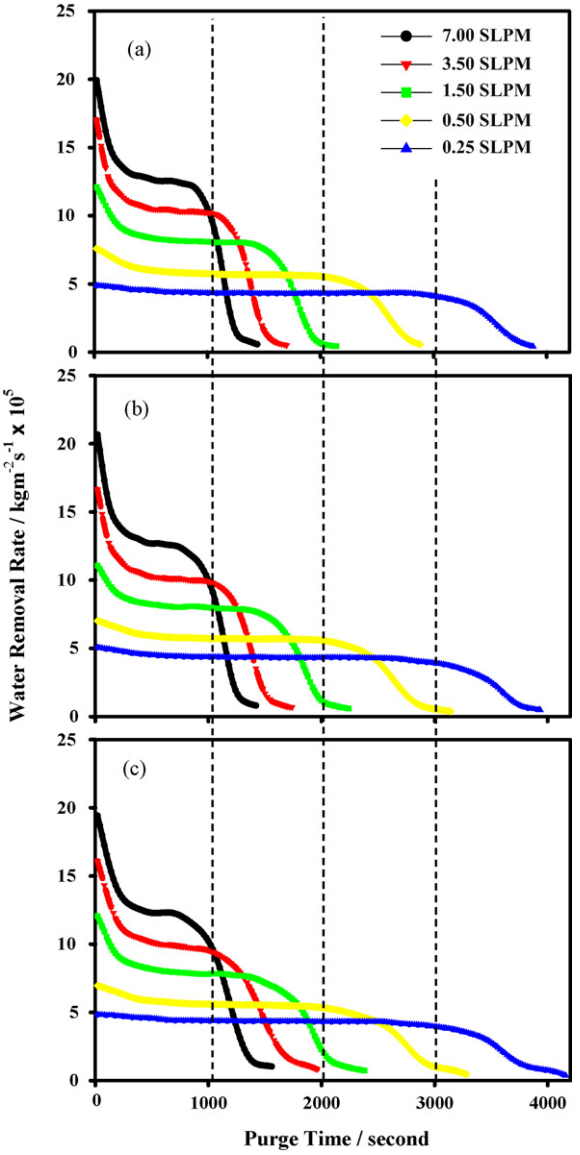

Fig. 2. Comparison of evaporative water removal rates: (a) for 10AC (0 wt% PTFE), (b) for 10CC (10 wt% PTFE), and (c) for 10DC (20 wt% PTFE) at various flow rates.

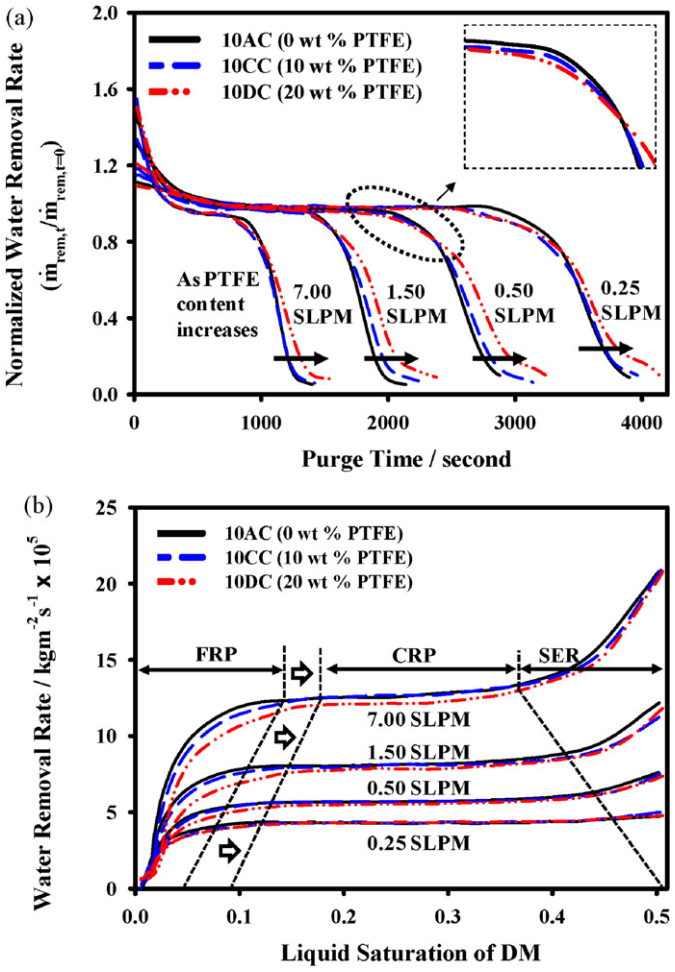

Fig. 3. Effect of PTFE content in DM on evaporative water removal rates: (a) normalized water removal rate with respect to purge time and (b) water removal rate with respect to saturation level of DM: arrows indicate that transition points from CRP to FRP occurred at higher saturation levels as PTFE content increases.

transition took place much more slowly (see Fig. 3(b)). This resulted in a prolonged gas purge to reach a non-saturated condition, as shown in Fig. 3(a).

The effect of geometric pore structure was also investigated. The water removal rate was compared with respect to purge time at various purge gas flow rates, as shown in Fig. 4. The required purge time increased from 24AA DM, to Carbel CL, and 10AC, as shown in Table 1. The difference in the initial water amount in each DM was normalized by dividing by the maximum amount of storable water in each DM calculated from Eq. (2), and water removal behaviors were compared with respect to saturation level of DM, as shown in Fig. 5.

As shown in Fig. 5(a), the CRP regime (plateau region of Fig. 5(b) and (c)) could not be achieved at higher gas purge flow rates for 2D structured DM (i.e. paper-type DM.), whereas the CRP regime became constant, extending into lower saturation level as DM pore structure became three-dimensional (i.e. cloth type DM). This means that for 2D pore structured DM, internal liquid flow from the main body of DM to the evaporation front on the surface of DM was not fast enough to match the water removal at the evaporating front. Therefore, the evaporation front penetrated into the DM even at higher saturation, leaving a higher saturation level to be removed in the more slowly evaporating FRP regime. The internal liquid transport was well-developed for 3D structured DM, consequently extending the CRP regime into lower saturation levels, leading to a more rapid water removal rate, and more efficient purge. This explains the observed superior drainage and purge characteristics of cloth-based DM. Region (R) in Fig. 5 indicates water removal behavior at the end of gas purge. It was found that for a 2D structure DM, some residual water remained in the DM and complete water removal was not achieved. As the structure of DM changed from 2D to 3D, however, complete water removal could be obtained. It should be noted that a complete dry-out of DM is not achieved or desired in actual fuel cell condition. However, the water removal behavior for complete dry-out can be utilized to better understand the impact of different pore structures on water removal. It also should be noted that 24AA DM does not have a micro-porous layer (MPL) whereas other DM such as 10AC and Carbel CL have MPLs. That may cause the water removal behavior of 24AA to differ from other DM due to the different wetting effects experienced between DM and test fixtures. This possibility was experimentally evaluated by inserting an MPL between the bottom of the 24AA and top of the sample holder. The evaporation behavior observed was found to be similar, indicating the MPL did not play a dominating role in the observed behavior.

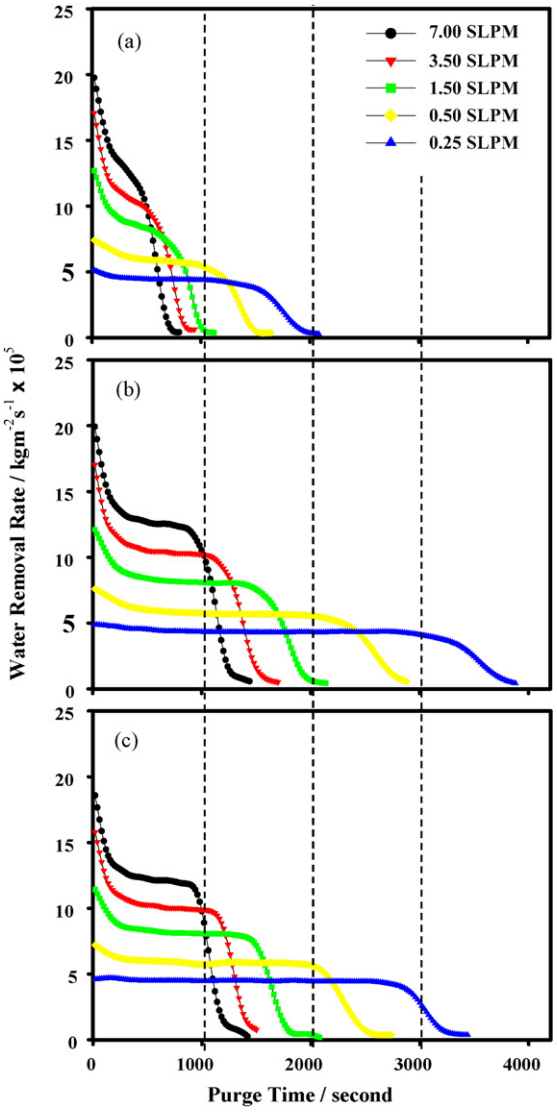

Fig. 4. Comparison of evaporative water removal rates: (a) for 24AA (2D pore structure), (b) for 10AC (partial 3D pore structure), and (c) for Carbel CL (3D pore structure) at various flow rates.

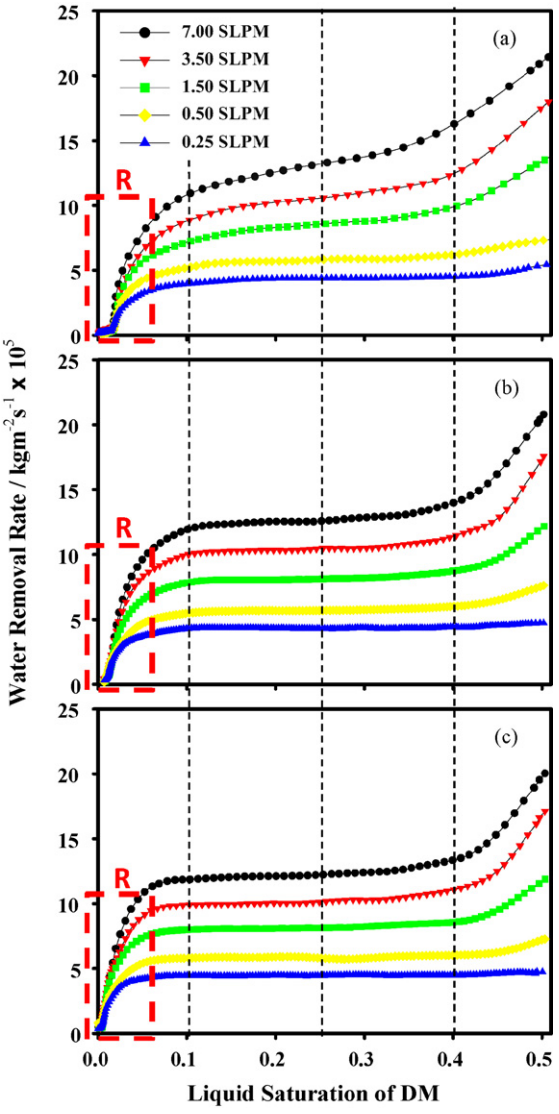

Fig. 5. Comparison of pore structure effect on evaporative water removal rates with respect to saturation level of DM: (a) for 24AA (2D pore structure), (b) for 10AC (partial 3D pore structure), and (c) for Carbel CL (3D pore structure). Region (R) indicates water removal behavior at the end of gas purge.

The general evaporation behavior can be further analyzed and understood with respect to the funicular regime and pendular regimes [21]. In the funicular regime, a continuous liquid film is connected through the porous matrix, and water removal rate is dominated by internal liquid flow. Therefore, the measured water removal in this regime can be utilized for analyzing the impact of material properties on internal capillary liquid flow rates and formation of hydraulic connectivity among pores. In contrast, water distribution in the pendular regime is characterized by discrete liquid water droplets, thus evaporation is dominated by vapor diffusion, and the impact of the DM properties can be analyzed primarily as a function of tortuosity. In the following sections, an analysis was conducted for both regimes.

3.2. Internal liquid water flow in DM

The water removal rate at the transition point from CRP to FRP regimes can be utilized to obtain the internal flow rate of liquid water for each DM during evaporation. As shown in Fig. 6(a), at this critical point the evaporative water removal rate at the open boundary is exactly balanced with internal liquid water transport rate. From evaporation plots, internal liquid flow rates for various saturation levels were obtained, and utilized to investigate the effect of PTFE content in Fig. 6(b) and geometric pore structure in Fig. 6(c).

As shown in Fig. 6(b), internal capillary liquid flow obtained experimentally in this study began only when saturation was above a certain level (which is called the irreducible saturation) and increased in a nonlinearly increasing way at the saturation level from 0.13 to 0.16, as reasonably expected from Refs. [21–24].

As DM PTFE content increased, the saturation level for the capillary flow rate increased, as shown in Fig. 6(b). When liquid water perfectly wets the surface pores in DM, hydraulic connections among pores can be maintained until low saturation of DM, and through the hydraulic connections, liquid water can be transported to the open boundary where evaporation takes place. However, when liquid water does not wet the surface of pores and forms discrete liquid droplets on surfaces, liquid connection among pores cannot be maintained without higher saturation levels.

The effects of geometric pore structures are compared in Fig. 6(c). The internal capillary flow rate significantly increased when saturation was above 0.08–0.15. Additionally, the internal

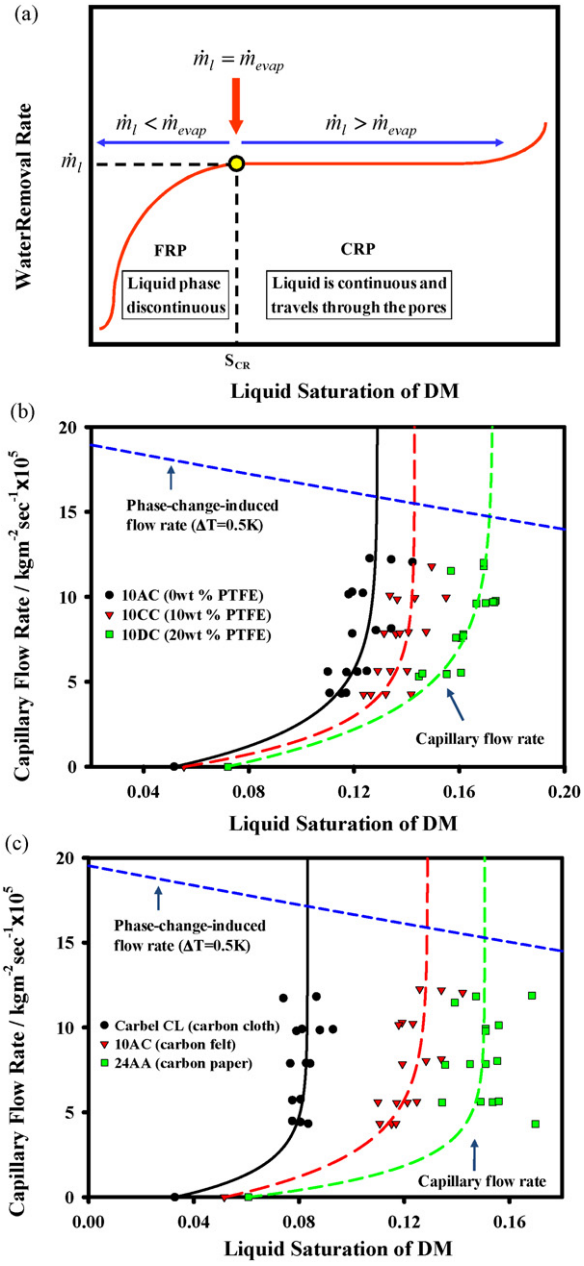

Fig. 6. Internal capillary liquid flow rate for water drainage during evaporation and comparison of capillary flow rate and phase-change-induced flow rate: (a) method to obtain the liquid flow rate, and comparison of effect of PTFE content in DM (b) and effect of pore structure (c) on internal capillary flow rate, respectively.

liquid water flow rate increased as pore structure changed from 2D to 3D geometry. For a 2D pore structured DM, carbon fibers are primarily aligned in x and y directions, as shown in Fig. 1(a). The pore matrix consists of multiple fiber layers in the in plane direction, and lacks through-plane pathways for drainage. However, the 3D pore structured DM has fibers aligned in x, y and z direction, and pore matrix is less tortuous, as shown in Fig. 1(c). Therefore, liquid water can move along with the aligned fibers out of DM efficiently for 3D pore structure DM.

The internal capillary flow rate obtained in this study can be further utilized to understand water transport behavior in an operating fuel cell. Water generated at the CL transports through DM to the flow field plate by capillary and phase-change-induced (PCI) modes [14,15,25]. The capillary flow is driven by a capillary pressure difference when liquid phase is connected through pores. PCI flow is driven by saturated vapor pressure gradient due to a temperature gradient [14]:

$$\vec{J}_{CP} = \rho_w k_{rw} \frac{k_w}{\mu_w} \nabla P_C \tag{3}$$

$$\vec{J}_{PCI} = \frac{D_{w,eff}}{R_v} \frac{d}{dT} \left(\frac{P_{sat}(T)}{T} \right) \nabla T \tag{4}$$

where $\vec{J}_{CP}$ is the capillary water flux, and ρ_w, k_{rw}, k_w, μ_w, and P_C are water density, water relative permeability, water absolute permeability, water viscosity, and capillary pressure, respectively. $\vec{J}_{PCI}$ is water flux by PCI mode, and $D_{w,eff}$, R_v, and P_{sat} are effective diffusivity of vapor, vapor gas constant, and saturation pressure, respectively.

$$D_{w,eff} = [\varepsilon(1-s)]^{3/2} D_w \tag{5}$$

$$D_w = D_w(T_{ref}, P_{ref}) \left(\frac{T}{T_{ref}} \right)^{3/2} \left(\frac{P_{ref}}{P} \right) \tag{6}$$

where ε and s are porosity and saturation of DM, respectively. D_w, T_{ref}, and P_{ref} are binary diffusion coefficient of water vapor in the air, reference temperature, and reference pressure, respectively.

The water transport via these two modes is compared in Fig. 6(b) and (c) with respect to liquid saturation of the DM. PCI flow through the DM was calculated using a simple 1D approximation for a temperature gradient of 0.5 K, which is typical at operation between 0.1 and 0.2 A cm^{-2} [26]. As shown in Fig. 6(b) and (c), PCI flow rate decreases as the saturation of DM increases due to decreasing porous space for vapor transfer, whereas capillary flow rate increases with saturation of DM due to increasing hydraulic connections among pores for liquid water to transport. PCI flow is based on bi-molar molecular diffusion, whereas capillary flow is a result of bulk liquid flow, and therefore it increases from negligible to much greater than PCI flow when the liquid phase is fully connected through pores. As shown in Fig. 6(b) and (c), PCI flow dominates in a lower saturation regime (i.e. below saturation of 0.09 for carbon cloth DM and from 0.13 to 0.17 for carbon paper DM). Above this saturation, capillary flow dominates. This behavior is also consistent with the experimental results of neutron radiography (NR) [27].

As discussed in Ref. [27], water saturation in DM increases gradually with time during operation at 0.2 A cm^{-2}, and reaches a peak water content in the DM. This supports the theory that the PCI flow is dominant mode at lower saturation, leading to increase of water amount in DM. As the water saturation approaches a certain level at which liquid connections among pores are fully developed and fast capillary liquid flow is generated, capillary flow becomes dominant, resulting in the peak observed. Ref. [27] also showed that at 1 A cm^{-2}, the DM approached the same steady saturation value, but much faster than at lower currents. Even though the high current operation (i.e. 1 A cm^{-2}) has approximately six times greater water transport rate by PCI mode than for low current operation (i.e. 0.2 A cm^{-2}), the steady-state distribution of liquid water was almost identical, indicating the dominance of capillary flow mode after the critical saturation level where connected pathways are formed. The maximum water amount at steady condition is around 120 mg cm^{-3} which corresponds to a DM saturation of 0.15 (SGL 10BB which is carbon felt type DM) [27].

Based on comparison of observed capillary flow to PCI flow at 1 A cm^{-2}, it can be concluded that PCI flow is dominant at lower saturation of DM, whereas capillary flow is dominant above the critical saturation level.

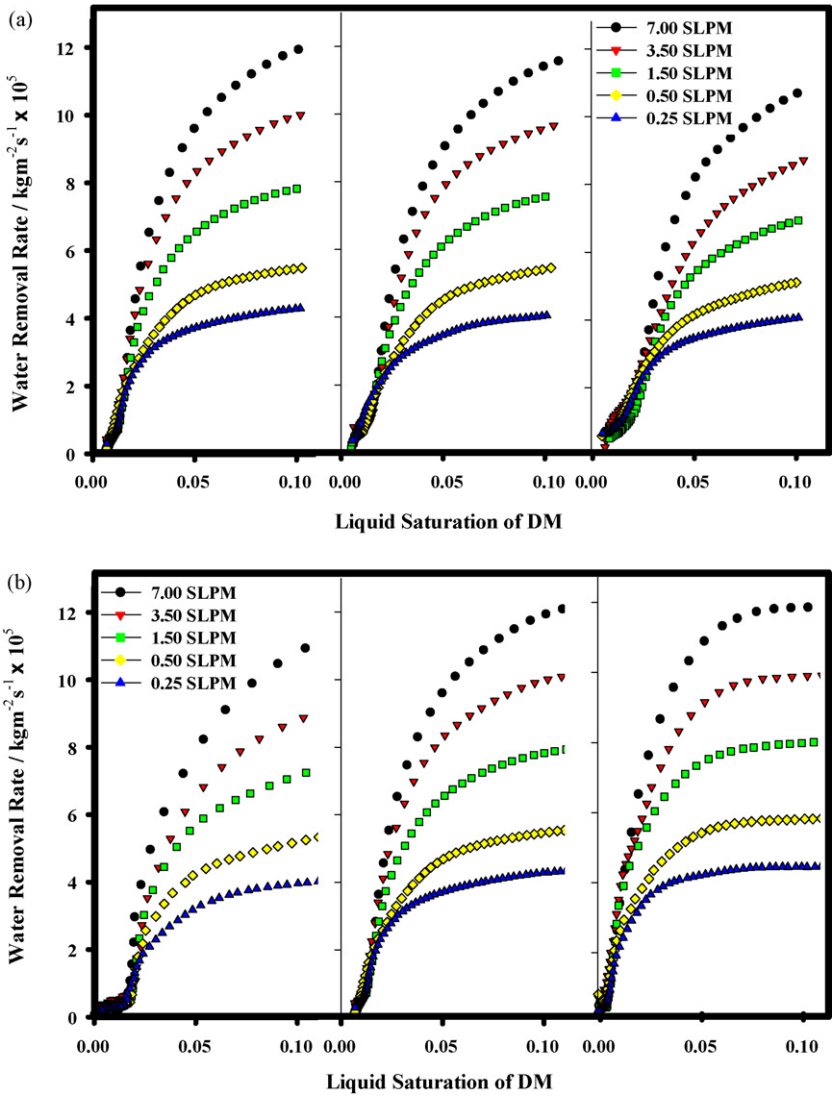

Fig. 7. Comparison of water removal rate in FRP regime: (a) effect of PTFE content (0, 10, and 20 wt% from left to right figures) and (b) effect of pore structure (2D, partial 3D, and 3D pore structure from left to right figures).

3.3. Diffusive water removal in falling rate period (FRP) regime

The evaporation front penetrates into the DM in the FRP regime, and vapor diffusion dominates water removal. Therefore, water removal in the FRP regime can be described with effective diffusivity and water vapor concentration, as shown in Eq. (7) for a one-dimensional system. Effective diffusivity is function of saturation and tortuosity representing the effect of porosity and DM geometric pore structure. And the surface area of water and gradient of water vapor concentration are functions of saturation. Those functional relations can be lumped into functions of saturation and tortuosity. Finally, the water removal rate can be described with respect to saturation, tortuosity, and a diffusive water removal relation:

$$\begin{aligned}\dot{m}_{w,rem} &= D_{w,eff} M_w A_s \frac{dc_w}{dz} \\ &= D_{w,eff}(s, \tau(\xi, \varepsilon)) M_w A_s(s) \frac{dc_w(s)}{dz(s)} \\ &\sim f(s) g(\tau) D_w M_w A_s \frac{dc_w}{dz}\end{aligned} \tag{7}$$

where $D_{w,eff}$ is effective diffusion coefficient of water to air, M_w is molecular weight of water, A_s is surface area of liquid water and dc_w/dz is gradient of water vapor concentration with respect to depth of DM, s is saturation level of DM, τ is tortuosity factor, ξ is pore geometry factor, ε is porosity, and D_w is diffusion coefficient of water to air.

This equation indicates the tortuosity is one of the key parameters for governing water removal rate in the FRP regime for a prescribed saturation level. Tortuosity represents the combined effect of different material properties of DM due to different PTFE content and pore geometric structure.

In Fig. 7(a) and (b), water removal behavior is shown for the FRP regime (saturation range from 0.1 to 0). As PTFE content in the DM decreased and pore structure changed from two to three dimensional, water removal rate increased, and the slope of the water removal rate with respect to saturation became steeper, which indicates water removal efficiency is greater for DM with less PTFE content and a three-dimensional pore structure. Those effects of PTFE content and pore structure of DM can be described with tortuosity. Tortuosity of each DM are compared in Table 1, where empirical relations [28] were utilized for calculation of tortuosity for macro-porous layer portion to understand the effect of PTFE content and porous structure, as described in Appendix A. As tortuosity increased, water removal rate was found to decrease in Fig. 7, validating the concept that the tortuosity in Eq. (7) is the key parameter representing the effects of material properties DM (PTFE

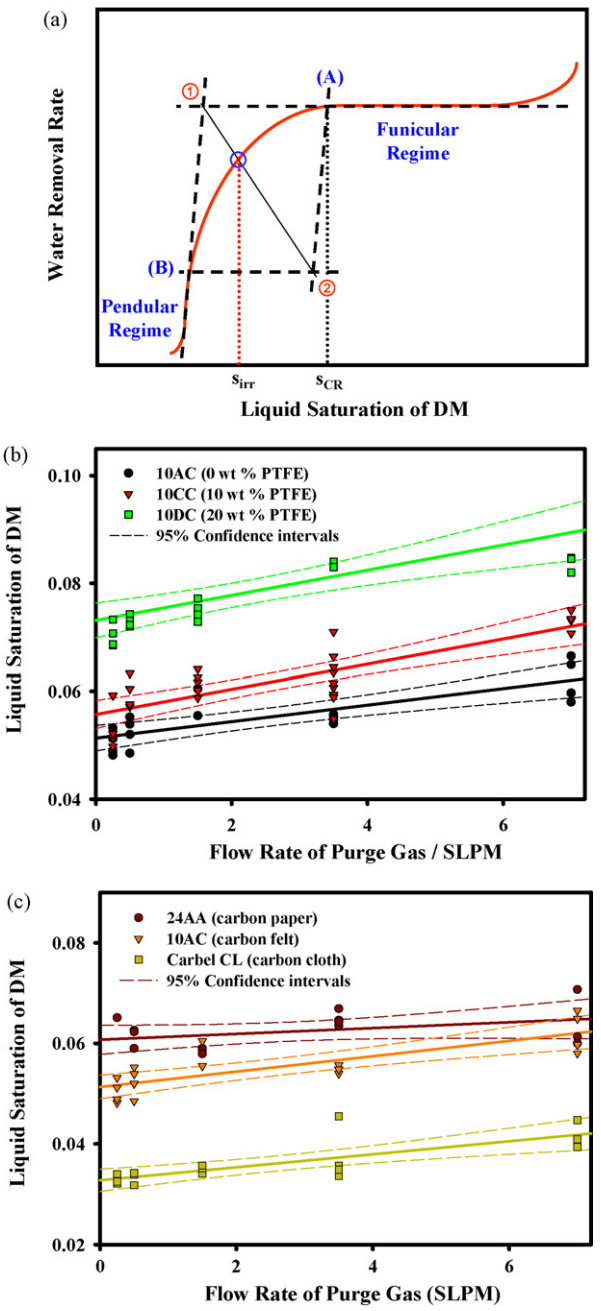

Fig. 8. Irreducible saturation of DM: (a) illustration of method to obtain the irreducible saturation, and comparison of effect of PTEF content (b) and effect of pore structure (c) on irreducible saturation, respectively.

content and pore structure). The effect of DM tortuosity on water removal rate also agrees with the results of Wang et al. [13].

3.4. Novel method to measure irreducible saturation

Irreducible saturation is the saturation level at the transition between funicular and pendular regimes. Almost no water can be drained by capillary mode below this saturation [22,23]. Therefore, this parameter is critical for modeling and simulation of multiphase flows including evaporation and condensation. In this study, a new method is introduced to obtain the irreducible saturation from the evaporation curve by utilizing a concept described by Kaviany et al. [21,24].

As shown in Fig. 8(a), two tangent lines are extended from each CPR and FRP regime, and intersection point (1) between two extended lines is connected to the other intersection point (2) between lines which have same slopes as the above extended lines and one of them going through points at the end of funicular regime (A) and the other through points at the start of full pendular regime (B), respectively. The newly connected line between point (1) and point (2) forms an intersection, which is a point where isolated droplet evaporation is dominant, and therefore is considered to be the irreducible point. From the experiment, the irreducible saturations were obtained at various flow rates. The intrinsic irreducible saturation was obtained by extrapolating the nominal irreducible saturation obtained at each flow rate to the zero flow rate condition, as shown in Fig. 8(b) and (c):

$$s_{irr} = \lim_{\dot{m}\to 0} s_{irr,\dot{m}} \tag{8}$$

where s_{irr} is the irreducible saturation of DM and $s_{irr,\dot{m}}$ is the nominal irreducible saturation obtained at each flow rate.

Irreducible saturations were found to be increased as PTFE content in the DM increased, which is same trend as the results of Gostick et al. [19] where s_{irr} was 0.04 and 0.07 for DM without PTFE content and with 5 wt% PTFE content, respectively. Irreducible saturations also increased as geometric pore structure changed from three to two dimensions, as shown in Fig. 8(b) and (c), respectively. These values are in the same range of results of Fairweather et al. [18] and Gostick et al. [19]. The irreducible saturation of DM was also found to vary with geometry of flow field in actual fuel cell system [29]. Depending on the area ratio of land to channel, the irreducible saturation was varied because the amount of immobile water resided under the land varies with the ratio. Therefore, the irreducible saturation (s_{irr}) obtained in this study can be considered as an intrinsic material property of DM which is not affected by the system.

It should be noted that the nominal irreducible saturation obtained at each flow rate was found to increase as flow rate of purge gas increased, as shown in Fig. 8(b) and (c). And therefore, this behavior can be utilized for designing advanced purge protocols.

3.5. Consideration of PTFE and pore structure effect on purge efficiency

The critical purge time (t_{CR}) was normalized by dividing with end of purge time (t_{End}) to understand purge efficiency in terms of utilization of applied purge time, as shown in Fig. 9. If normalized critical purge time (t_{NCR}) is high, it indicates a much greater portion of the purge time is utilized for water removal in SER and CRP regime where water removal is achieved faster and more efficiently.

As PTFE content increased and geometric pore structure changed from 3D to 2D, t_{NCR} decreased, indicating purge efficiency decreased, as shown in Fig. 9(b) and (c), respectively. A lower flow rate of gas was found to be more efficient in terms of utilization of applied purge time.

3.6. Guideline for effective purge

Optimized purge is obtained with minimal time and energy, and low moisture gradients across the membrane. In order to remove water from DM effectively and durably, most water should be removed in the CRP regime. This can be achieved through use of mixed flow rates approach [17]. Water slugs residing in flow channel or on the DM can be efficiently removed by a brief high flow rate purge. Then, with a gradually decreasing flow rate, the hydraulic connections among pores can be maintained until the lowest possible saturation level, providing an efficient purge that reduces

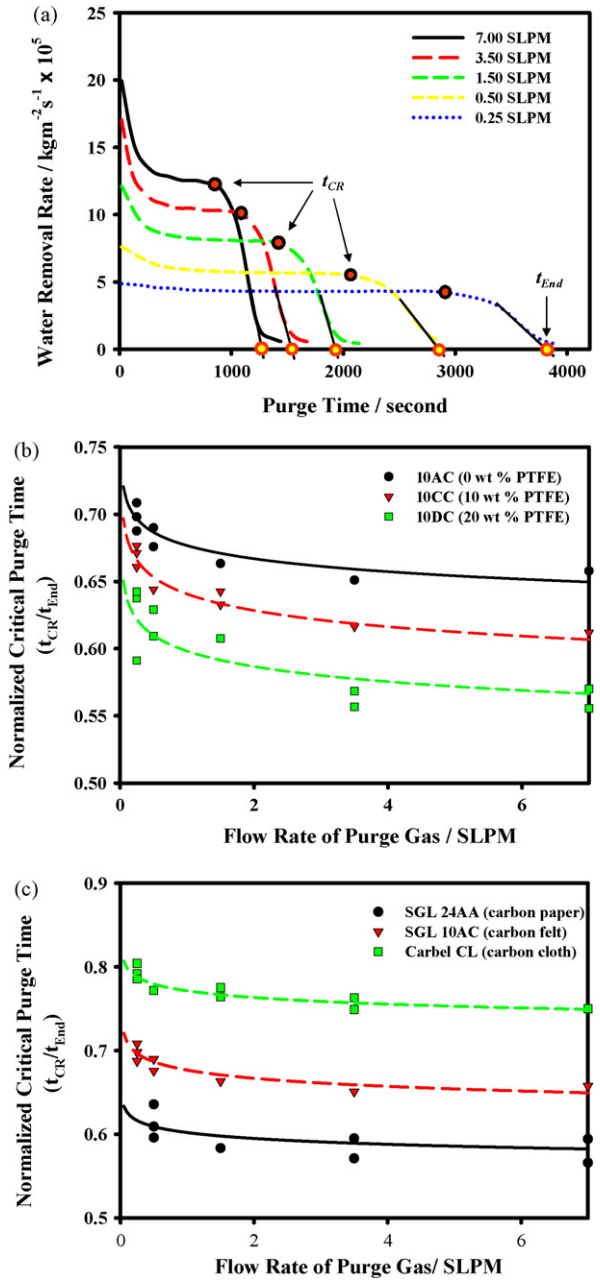

Fig. 9. Purge effectiveness at the critical condition: (a) water removal versus time, (b) impact of PTFE content on normalized critical purge time and (c) impact of DM material on normalized critical purge time.

membrane moisture gradients that have been shown to negatively impact durability [29]. The internal liquid flow rate (capillary flow rate) through hydraulic connections among pores was found to increase as PTFE content decreased and pore structure changed to 3D structure, as described. Therefore, the effective and durable purge can be achieved by fully utilizing the benefit of water removal in CRP regime by applying a composite flow rate and DM with less hydrophobic treatment and 3D fiber matrix structure. Obviously, this may lead to performance trade-offs in normal operation.

4. Summary and conclusions

The effects of polytetrafluoroethylene (PTFE) content in diffusion media (DM) and geometric pore structure on evaporative water removal from DM were investigated in this work. Additionally, new methods to determine internal liquid flow rate and irreducible saturation were discussed. The following conclusions are drawn from this study.

- The internal capillary flow rate was found to increase as PTFE content decreased and geometric pore structure changed from two to three dimensional in nature. In operation, phase-change-induced flow was a dominant mode of transport for saturation below 0.09 for carbon cloth type DM and below 0.12 for carbon paper-type DM. Above these saturation levels, capillary flow is dominant.
- A new method to measure the irreducible saturation was developed, and the irreducible saturation was obtained in the range from 0.03 to 0.07, which increased as PTFE content in DM increased and pore structure changed from three to two dimensional in nature.
- The effect of PTFE and pore structure on water vapor diffusion was investigated in the FRP regime where vapor diffusion is dominant mode for water removal. Tortuosity was found to be a key material property to control the vapor diffusion.
- Water removal efficiency was compared with normalized critical purge time, and was found to increase as PTFE content decreased and geometric pore structure changed to three dimensions, indicating that although PTFE is helpful to avoid flooding during normal operation, it can reduce purge efficiency during shutdown.

Acknowledgments

The authors thank Prof. John Cimbala of Pennsylvania State University for helpful advice, Dr. B.K. Hong of Hyundai and Kia Motors for providing samples of diffusion media, M. Hatzell of FCDDL for fruitful discussion, and Dr. Daniel S. Hussey and Dr. David L. Jacobson at NIST for arranging beam availability and helpful advice. Prof. Mench acknowledges financial support by the National Science Foundation CAREER Award (CBET #-0644811).

Appendix A. Calculation of porosity of macro-porous layer of DM

The porosity of the macro-porous layer of DM was calculated from following equations [30]:

$$\varepsilon_{macro} = \frac{V_{macro,p}}{V_{macro}} = \frac{\varepsilon_t V_t - \varepsilon_{MPL} V_{MPL}}{V_{macro}} \quad (A.1)$$

$$\varepsilon_{MPL} = (1 - r_{p,V})\varepsilon_t \frac{t_t}{t_{MPL}} \quad (A.2)$$

$$r_{P,V} = \frac{V_{macro,p}}{V_{t,p}} \quad (A.3)$$

where ε_{macro} is porosity of macro-porous layer of DM, $V_{macro,p}$ is pore volume of macro-porous layer, V_{macro} is volume of macro-porous layer, ε_t and V_t are total porosity and total volume of DM including macro-porous layer and micro-porous layer (MPL), respectively, ε_{MPL} and V_{MPL} is porosity and volume of MPL, $r_{p,V}$ is ratio of pore volume of macro-porous layer to pore volume of total DM ($V_{t,p}$), t_t and t_{MPL} are thickness of total DM and thickness of MPL, respectively.

To obtain MPL porosity, SGL 10BA and 10BC were utilized, which have same type of macro-porous layer, but only 10BC has MPL. Thickness and porosity of SGL 10BA were 0.32 mm and 0.88, respectively whereas 10BC has 0.42 mm in thickness and 0.82 in porosity, respectively. By utilizing the thickness of MPL which found to be 0.1 mm in SEM images, $r_{p,V}$ and porosity of MPL were determined to be 0.81 and 0.63 from Eqs. (A.3) and (A.2), and the porosity of macro-porous layer of each tested DM was calculated from Eq. (A.1) under the assumption that same type of MPL was applied to SGL

10AC, 10CC, and 10DC. As shown in Table 1, the calculated porosity of macro-porous layer of DM was reasonable by comparison of the porosity of 10BA, which has 5 wt% PTFE without MPL. For porosity of MPL of Carbel CL, value of 0.05 was utilized, which was provided from manufacturer. The tortuosity of the macro-porous layer of DM was calculated from equation:

$$\tau = \varepsilon N_m \tag{A.4}$$

where τ is tortuosity, ε is porosity, and N_m is MacMullin number, $N_m = \varepsilon^{-3.8}$ and $\varepsilon^{-1.5}$ for carbon paper DM and carbon cloth DM, respectively [28].

References

[1] J. St-Pierre, J. Roberts, K. Colbow, S. Campbell, A. Nelson, J. New Mater. Electrochem. Syst. 8 (2005) 163–176.
[2] K.T. Cho, A. Turhan, J.H. Lee, J.S. Brenizer, A.K. Heller, L. Shi, M.M. Mench, Nucl. Instrum. Methods Phys. Res., Sect. A 605 (2009) 119–122.
[3] C. Quick, D. Ritzinger, W. Lehnert, C. Hartnig, J. Power Sources 190 (2009) 110–120.
[4] N. Shahidzadeh-Bonn, A. Azouni, P. Coussot, J. Phys.: Condens. Matter 19 (2007) 112101.
[5] E.C. Kumbur, K.V. Sharp, M.M. Mench, J. Electrochem. Soc. 154 (2007) B1295–B1304.
[6] E.C. Kumbur, K.V. Sharp, M.M. Mench, J. Electrochem. Soc. 154 (2007) B1305–B1314.
[7] E.C. Kumbur, K.V. Sharp, M.M. Mench, J. Electrochem. Soc. 154 (2007) B1315–B1324.
[8] J.T. Gostick, M.A. Ioannidis, M.W. Fowler, M.D. Pritzker, J. Power Sources 194 (2009) 433–444.
[9] J.D. Fairweather, P. Cheung, D.T. Schwartz, J. Power Sources 195 (2010) 787–793.
[10] M. Mathias, J. Roth, J. Fleming, W. Lehnert, in: W. Vielstich, H.A. Gasteiger, A. Lamm (Eds.), Handbook of Fuel Cells—Fundamentals, Technology and Applications, vol. 3, John Wiley & Sons, Ltd., New York, 2003, pp. 517–537, Part I, Chapter 46.
[11] J. Zhang, D. Kramer, R. Shimoi, Y. Ono, E. Lehmann, A. Wokaun, K. Shinohara, G.G. Scherer, Electrochim. Acta 51 (2006) 2715–2727.
[12] J.J. Kowal, A. Turhan, K. Heller, J. Brenizer, M.M. Mench, J. Electrochem. Soc. 153 (2006) A1971–A1978.
[13] Y. Wang, C.-Y. Wang, K.S. Chen, Electrochim. Acta 52 (2007) 3965–3975.
[14] M. Khandelwal, S. Lee, M.M. Mench, J. Electrochem. Soc. 156 (2009) B703–B715.
[15] S. Kim, M.M. Mench, J. Electrochem. Soc. 156 (2009) B353–B362.
[16] R. Bradean, H. Haas, K. Eggen, C. Richards, T. Vrba, ECS Trans. 3 (2006) 1159–1168.
[17] K.T. Cho, M.M. Mench, J. Power Sources 195 (2010) 3858–3869.
[18] J.D. Fairweather, P. Cheung, J. St-Pierre, D.T. Schwartz, Electrochem. Commun. 9 (2007) 2340–2345.
[19] J.T. Gostick, M.A. Ioannidis, M.W. Fowler, M.D. Pritzker, Electrochem. Commun. 10 (2008) 1520–1523.
[20] O. Chapuis, M. Prat, M. Quintard, E. Chane-Kane, O. Guillot, N. Mayer, J. Power Sources 178 (2008) 258–268.
[21] J.A. Rogers, M. Kaviany, Int. J. Heat Mass Transfer 35 (1992) 469–480.
[22] S. Litster, N. Djilali, in: B. Sunden, M. Faghri (Eds.), Transport Phenomena in Fuel Cells, WIT Press, UK, 2005, pp. 175–213, Chapter 5.
[23] M. Kaviany, Principles of Heat Transfer in Porous Media, second ed., Springer, 1995.
[24] M. Kaviany, M. Mittal, Int. J. Heat Mass Transfer 30 (1987) 1407–1418.
[25] A.Z. Weber, J. Newman, J. Electrochem. Soc. 153 (2006) A2205–A2214.
[26] M. Khandelwal, M.M. Mench, J. Power Sources 161 (2006) 1106–1115.
[27] A. Turhan, S. Kim, M. Hatzell, M.M. Mench, Electrochim. Acta 55 (2010) 2734–2745.
[28] M.J. Martinez, S. Shimpalee, J.W. Van Zee, J. Electrochem. Soc. 156 (2009) B80–B85.
[29] K.T. Cho, Ph.D. Dissertation, The Pennsylvania State University, 2010.
[30] J.T. Gostick, M.W. Fowler, M.A. Ioannidis, M.D. Pritzker, Y.M. Volfkovich, A. Sakars, J. Power Sources 156 (2006) 375–387.